Photochemistry and Photobiology, 2007, 83: 263–272

Analysis of Light-Induced Conformational Changes of *Natronomonas pharaonis* Sensory Rhodopsin II by Time Resolved Electron Paramagnetic Resonance Spectroscopy†

Enrica Bordignon[1], Johann P. Klare[1,2], Julia Holterhues[1], Swetlana Martell[2], Aliaksei Krasnaberski[1], Martin Engelhard[2] and Heinz-Jürgen Steinhoff*[1]

[1]Fachbereich Physik, Universität Osnabrück, Osnabrück, Germany
[2]Max-Planck-Institut für Molekulare Physiologie, Dortmund, Germany

Received 5 July 2006; accepted 29 August 2006; published online 7 September 2006 DOI: 10.1562/2006-07-05-RA-960

ABSTRACT

The nature and kinetics of the conformational changes leading to the activated state of *Np*SRII/*Np*HtrII$_{157}$ were investigated by time-resolved electron paramagnetic resonance (TR-EPR) spectroscopy in combination with site-directed spin labeling (SDSL) on a series of spin labeled mutants of *Np*SRII. A structural rearrangement of the cytoplasmic moiety of *Np*SRII upon light activation was detected (helices B, C, F and G). The increase in distance between helices C and F in the M-trapped state of the complex observed in one double mutant is in line with the notion that an outward movement of helix F occurs upon receptor activation. The data obtained from the *Np*SRII/*Np*HtrII$_{157}$ complex reconstituted in purple membrane lipids are compared with those obtained from the X-ray structure of the late M-state of the complex which shows some discrepancies. The results are discussed in the context also of other biophysical and EPR experimental evidences.

INTRODUCTION

In halophilic archaea like *Halobacterium salinarum* and *Natronomonas pharaonis* (*Np*), the photophobic response to green-blue light is mediated by sensory rhodopsin II (SRII, also named phoborhodopsin) (for recent reviews see [1–5]). SRII is structurally and functionally closely related to the light driven ion pumps bacteriorhodopsin (BR) and halorhodopsin (HR). These proteins comprise seven transmembrane helices (A–G) and a retinal chromophore covalently bound via a protonated Schiff base to a conserved lysine residue on helix G. The signal transduction to the intracellular two-component pathway, which modulates the swimming behavior of the cell, is accomplished by the interaction with the tightly bound transducer protein HtrII (halobacterial transducer) in a 2:2 complex. A transducer dimer, comprising a transmembrane domain and a cytoplasmic signaling/adaptation domain connected by a linker region, binds two receptor proteins within the membrane. Photo-excitation of the receptor protein (λ_{max} = 500 nm for *Np*SRII) induces a photocycle similar to that of bacteriorhodopsin with the photocycle intermediates labeled K, L, M, N and O. The analysis of this photocycle revealed a spectrally silent irreversible transition between two M-states (M_1 and M_2) with a time constant of 3 ms (6). The initial step of the photocycle is the isomerization of the retinal chromophore from all-*trans* to 13-*cis*, thereby triggering a series of conformational changes, which finally lead to activation of the bound transducer dimer. The nature and kinetics of these conformational changes were investigated by time-resolved electron paramagnetic resonance (TR-EPR) spectroscopy in combination with site-directed spin labeling (SDSL). Analysis of the data obtained with the *Np*SRII reconstituted in purple membrane lipids (PML) in the absence of transducer revealed a transient mobilization of the spin label side chain at residue S158R1^F (located at the outwardly oriented face of helix F) and residue L159R1^F (located at the F–G helices interface) in the cytoplasmic moiety of helix F (see Fig. 1 for position of spin labels), thus suggesting a light-induced displacement of the latter. On the other side, for helix G EPR data suggest just minor light-induced structural rearrangements with respect to the other neighboring helices. Analysis of the data obtained with the *Np*SRII reconstituted in PML in the presence of the transducer (2:2 complex) revealed that, in contrast to the results of the transducer-free samples, the spin label side chain S158R1^F became transiently less mobile during the photocycle (S158R1^F is located in the 2:2 complex at the F-TM2 interface). Contrarily, the increase in mobility detected for L159R1^F was still observable (7). Thus, the conformational change of helix F persists in the presence of the transducer. These observations were interpreted with an outward bending motion of the cytoplasmic half of helix F occurring during the M_1 to M_2 transition (5), and a recovery of its initial position with the reformation of the receptor ground (dark) state. This is in analogy to the motion of the corresponding helix in BR (8), which has been demonstrated by means of cryo-electron microscopy (9), X-ray structural analysis (10,11) and EPR spectroscopy (12,13). It was concluded that this conformational change of helix F triggers the activation of the transducer molecule, reflected in a rotary or screw-like motion of its second transmembrane helix (TM2) as revealed by EPR spectroscopy (14) and confirmed by X-ray structure analysis (15). However, the X-ray structure of the activated state of the receptor/transducer complex revealed no

†This paper is part of the Proceedings of the 12th International Conference on Retinal Proteins held at Awaji Island, Hyogo, Japan on 4–8 June 2006.
*Corresponding author e-mail: hsteinho@uos.de (Heinz-Jürgen Steinhoff)

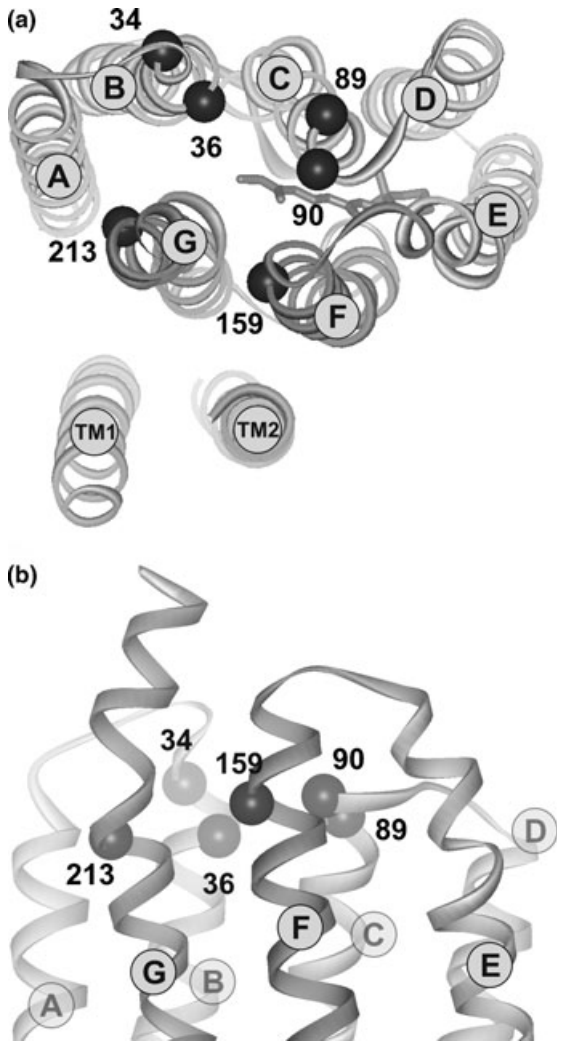

Figure 1. Crystal structure of the *Np*SRII/*Np*HtrII$_{114}$ complex (pdb: 1H2S) in ribbon representation. (a) View from the cytoplasmic side. (b) Side view of the receptor (transducer helices are omitted for clarity). The C_α atoms of the amino acids that where replaced by cysteines and modified with the MTS spin label are indicated.

significant conformational changes for helix F, whereas helix G was found to shift towards the extracellular side with respect to helix F by about 0.06 nm. Nevertheless, in agreement with the previously published EPR data, the signal transfer was suggested to involve interactions between helices F and G of the receptor and TM2 of the transducer, and a rotation of TM2 in the direction and with the same extent as concluded from the EPR data was observed.

To address the discrepancies between the transient EPR and the crystallographic data and to investigate the overall motion of the seven helices of *Np*SRII in the activated state, we studied the light-induced conformational changes in *Np*SRII in the 2:2 complex reconstituted in PML in more detail applying SDSL-EPR spectroscopy. In a set of experiments, similar to those carried out by Rink *et al.* for BR (12), we examined the conformational changes by analyzing light-induced changes in the mobility of the spin label side chains located at the cytoplasmic ends of helices F (L159R1^F, F–G interface), G (L213R1^G, G–A interface), B (R34R1^B, outwardly oriented; Y36R1^B, inwardly oriented) and C (L89R1^C, outwardly oriented; L90R1^C, inwardly oriented) (Fig. 1). Additionally, one double mutant with the spin label side chains on helices C (L89R1^C) and F (L159R1^F) was engineered to determine changes in the distances between this pair of helices (the superscripts are used also in the following to denote the helix where the side chain resides). The data are compared with the analogous EPR data obtained for BR and to the recently published crystallographic data for the excited state of the *Np*SRII/*Np*HtrII complex.

MATERIALS AND METHODS

Protein expression and spin labeling. Protein expressions, spin labeling and sample preparation by reconstitution in PML were carried out as described previously (7,14,16). For purification purposes all proteins have a C-terminal His-tag. The transducer construct was truncated at position 157 (*Np*HtrII$_{157}$). The double mutant of *Np*SRII for inter-spin distance measurements was prepared using the same protocol.

EPR cw setup. For room temperature (296–299 K) measurements, sample volumes of 15 μL were filled into EPR glass capillaries (0.9 mm inner diameter) at final concentrations of 15–20 mg mL^{-1}. The cw-EPR experiments were performed using a home-made EPR spectrometer equipped with a Bruker dielectric resonator. The microwave power was set to 1.0 mW, the B-field modulation amplitude was 0.15 mT. For the time-resolved experiments, a modulation amplitude of 0.33 mT was used to enhance the signal-to-noise ratio.

For low temperature cw-EPR experiments sample volumes of 40 μL were loaded into EPR quartz capillaries (3 mm inner diameter) at final concentrations of 15–20 mg mL^{-1}. Spectra were recorded at 170 K using a home-made EPR spectrometer equipped with an AEG H103 rectangular cavity, with the microwave power set to 0.2 mW. The B-field modulation amplitude was adjusted to 0.25 mT. A Bruker B-NM 12 B-field meter measured the B-field and a continuous flow cryostat Oxford ESR 900 allowed stabilization of the sample temperature. In order to trap the M-intermediate, the light of a 100 W halogen lamp (filtered with an OG 520 filter and a heat filter) was focused directly onto the sample tube in the resonator. The sample was illuminated during freezing from 273 to 180 K at a cooling rate of approximately 10 K min^{-1}.

Time-resolved EPR setup. For transient EPR experiments, an excimer pumped dye laser (Lambda Physik, Göttingen, Germany) tuned at a wavelength of 500 nm was used. The duration of the light pulse from the excimer was 20 ns (FWHM) and the energy per pulse measured at the sample location was 1.2 mJ. To avoid photobleaching, grey filters with optical densities of 0.3 or 0.6 were used additionally. The EPR transients were recorded for 4 s after the laser flash at fixed B-field positions. The transients consist of 4×10^4 points sampled at a rate of 10^4 s^{-1}. Between 10^3 and 10^4 EPR transients were averaged to obtain a good signal-to-noise ratio. In general, the amplitudes of the transient traces were in the order of 1% of the maximum intensity of the cw EPR spectrum. Despite the intrinsic difficulties in determining the number of excited molecules, it is possible to estimate that about 10–20% of the sample was excited by light under the experimental conditions used. The relative change of the EPR intensities can be therefore estimated to be in the range 5–10%. The integration time of a lock-in amplifier (Signal recovery, model 7225, Ametek GmbH, Meerbusch, Germany) was set to 10 ms for the detection of the difference spectra or 5 ms for the detection of the kinetics of the EPR signal changes.

Difference spectra between the photo-activated and the initial states were recorded by detecting the EPR transients at different B-field values corresponding to a B-field scan. The cw spectrum of the ground state was obtained concomitantly to the EPR transient traces by averaging the signal intensity detected during the 100 ms duration of the pre-trigger before the laser flash. The kinetics of the EPR signal changes were analyzed for selected B-field values where the difference spectra showed local extremes.

The formation of the activated complex is faster than the time resolution of the EPR setup used (5 ms), thus the EPR traces cover only the decay of the EPR signal after photo-excitation (*i.e.* the recovery of *Np*SRII to its initial state). The transient decay of the

EPR signals were fitted with exponential functions to obtain the approximate decay time constant. For the mutants presented, a mono-exponential decay was shown to fit the EPR traces satisfactorily.

Simulation of the EPR spectra. The simulation of the cw EPR spectra presented in Fig. 3b (bottom spectra) was performed according to the Brownian model of isotropic re-orientational diffusion of the nitroxide (17). To obtain a simulated difference spectrum, two spectra were calculated, using the same hyperfine (A_{xx} = 0.52 mT, A_{yy} = 0.45 mT, A_{zz} = 3.60 mT) and g tensor (g_{xx} = 2.0087, g_{yy} = 2.0066, g_{zz} = 2.0026) values but different reorientation correlation times of 21 and 17 ns, and subsequently subtracted.

Fitting of the simulated dipolar broadened EPR powder spectra to experimental spectra recorded at 170 K revealed the average inter-spin distance according to the method described in (18). In this study, a Gaussian distribution of the inter-spin distances is assumed with a fixed distribution width of 0.2 nm. During the fitting procedure, the g tensor values, the values of A_{xx} and A_{yy} of the hyperfine tensor and the line width parameters were fixed to the values found for the corresponding singly labeled species. The parameters used are g_{xx} = 2.0087, g_{yy} = 2.0067, g_{zz} = 2.0026, A_{xx} = 0.59 mT and A_{yy} = 0.40 mT. A_{zz} was variable to account for differences in the polarity of the spin label environment (13,19,20). The spectra were convoluted with a field-independent line-shape function composed of a superposition of 44% Lorentzian and 56% Gaussian of 0.28 and 0.36 mT width. In the case of double mutant L89R1^{C}/L159R1^{F}, the amount of the singly labeled species was set to 50% in accordance with the experimentally determined spin labeling efficiency.

The average inter-spin distance of a Gaussian distribution with 0.2 nm width was determined in the fitting procedure.

Flash photolysis setup. The experimental setup for the transient absorption measurements was as follows. A Nd–YAG laser (Continuum YG601, 35 ps, 532 nm, 1 mJ) was used for excitation. The light from a 100 W halogen lamp was filtered with IR-cut-off and a 500 nm interference filter and passed through the sample cuvette placed in a temperature-controlled sample holder with a temperature stability within 0.1 K. For detection, the transmission light was focused on the input slit of a monochromator and then detected with a photomultiplier. The signal was recorded on a digital oscilloscope. To improve the signal-to-noise ratio, 10^2 transient optical traces were averaged. The transient absorption changes were detected at 296 ± 0.5 K at 500 nm for *Np*SRII/*Np*HtrII$_{157}$ complexes reconstituted in PML at a concentration of about 1 mg mL^{-1}.

RESULTS

Figure 1 shows a model of the *Np*SRII structure (in complex with *Np*HtrII [15]) where those residues that were replaced by cysteine and subsequently labeled with the MTS ([1-oxyl-2,2,5,5-tetramethylpyrroline-3-methyl]methanethiosulfonate) spin label are indicated. Residue L159^{F} resides at the cytoplasmic end of helix F, and residue L213^{G} is located at the interface between helices G and A. Residues R34^{B} and Y36^{B} are located on helix B, and L89^{C} and L90^{C} on helix C, with the latter ones pointing into the interior of the protein. All EPR and optical measurements were carried out with the spin-labeled receptor mutant in complex with a transducer construct, truncated at position 157 (*Np*HtrII$_{157}$), which has previously been shown to represent a good model concerning the receptor/transducer interaction (21).

The cw EPR spectra detected at room temperature (23–26°C) for the sensory rhodopsin mutants under investigation are shown in Fig. 2. The features of the room temperature EPR spectra reflect the reorientational motion of the nitroxide side chain attached to the engineered cysteine residue. Spectra of mobile side chains are characterized by a narrow linewidth and a small apparent hyperfine splitting as a result of the fact that the anisotropic components of the g and hyperfine tensors

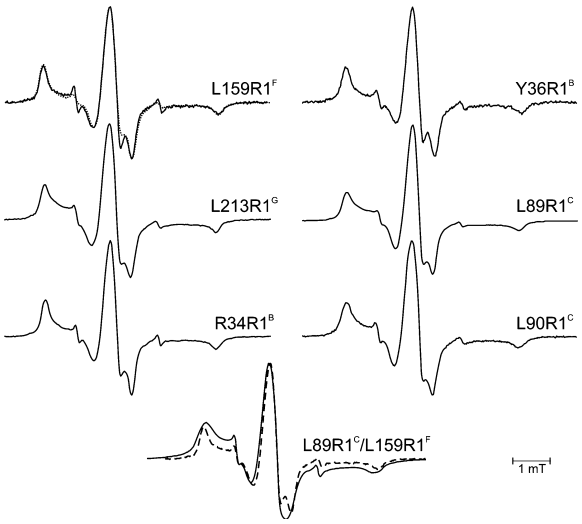

Figure 2. Room temperature first derivative cw electron paramagnetic resonance spectra of the MTS spin label attached to the indicated positions of the sensory rhodopsin *Np*SRII in complex with the transducer *Np*HtrII$_{157}$ reconstituted in purple membrane lipids (black lines). The spectra are scaled to equal positive amplitude of the central peak. The spectrum recorded for L159R1^{F} of *Np*SRII reconstituted in PML in the absence of *Np*HtrII (dotted line) is superimposed to the spectrum of L159R1^{F} in the 2:2 complex. At the bottom the dipolar broadened spectrum of the double mutant L89R1^{C}/L159R1^{F} (black line) is superimposed to the sum of the spectra of the corresponding singly labeled variants L89R1^{C} and L159R1^{F} (dashed line). Negligible amount of unbound spin label, which could not be eliminated by repetitive washing, is present in all spectra.

are averaged. In contrast to that, strong restrictions of the nitroxide motion caused by tertiary interactions result in line broadening and a larger apparent hyperfine splitting.

As expected, spin label side chains located in the protein interior (Y36R1^{B}, L90R1^{C}, L159R1^{F} and L213R1^{G}) exhibited strong restriction of the nitroxide reorientational motion. Surprisingly, the dynamics of L89R1^{C} and R34R1^{B}, both located at the outwardly oriented faces of helices B and C, respectively (see Fig. 1), were also strongly restricted, indicating either an interaction with the head groups of the lipid bilayer, or an orientation of the spin label side chain locating the nitroxide in between the receptor helices, or alternatively an interaction with adjacent receptor monomers in the membrane. Low temperature cw EPR spectra detected for these two single mutants in the receptors solubilized in β-dodecyl-D-maltoside (DDM) showed dipolar broadening indicating close contacts between helices B and C of adjacent monomers (not shown). Interestingly, such dipolar broadening was not observed for the L89R1^{C} and R34R1^{B} single mutants when the receptors were reconstituted with the transducer molecules.

At the bottom of Fig. 2 two spectra are superimposed, representing the sum of the spectra of the singly labeled L89R1^{C} and L159R1^{F} (dashed line) and the spectrum obtained from the doubly labeled variant of the two side chains (continuous line). The appearance of broadening that is visible in the spectrum of the doubly labeled variant indicates dipolar interaction. The distance between the two spins was determined for both the dark and the M-trapped state via low temperature EPR spectroscopy to monitor eventual changes in

the interactions between helices C and F upon light excitation (see below).

Transient changes of the nitroxide dynamics

In order to analyze the structural changes occurring in *Np*SRII upon light excitation, EPR difference spectra (activated-dark spectra) were monitored directly during a B-field scan (see Materials and Methods) for all mutants investigated (Fig. 3b). Considerable spectral changes were observed for all variants.

The transient spectra of L213R1^{G} and L89R1^{C} were characterized by relatively small amplitudes, indicating a minor structural change induced by light in the spin label micro-environment. In most of the variants, the spectral pattern of the difference spectra was in line with an increased mobility of the spin label upon light excitation. Figure 3a shows for each mutant a selected EPR transient trace (noisy grey line, time window 0.03–4 s) and the mono-exponential fitting (straight black line) utilized to extract the time constant of the decay of the structural changes occurring (see Table 1). Figure 3b presents the amplitudes of the transient traces detected at several B-field values (stick representation) which build up the difference spectrum. The difference spectra are superimposed to the cw EPR spectra detected concomitantly to the B-field sweep.

To discriminate between an increase and a decrease in the spin label mobility by inspection of the difference spectra (activated-dark state), attention is focused on the fingerprint spectral regions of the difference spectra at the low B-field peak and the central peak. In the case of an increase in mobility induced by light, one has to expect in the low B-field region a negative feature followed by a positive one. In the central peak of the spectrum this pattern is reversed, *i.e.* a positive narrow feature is followed by a negative band. Generally, the zero crossings of the difference spectrum and of the cw spectrum coincide. In case the mobility decreases upon light excitation, the inversed spectral changes are expected.

An example of a simulated difference spectrum characterized by a decrease in the spin label mobility is presented in Fig. 3b (bottom spectra). Two spectra characterized by the same hyperfine and *g* tensor values have been simulated, with correlation times of 21 and 17 ns. The correlation time of the "dark" simulated spectrum (17 ns) is in line with the highly restricted motion of the spin labels attached at the positions under investigation. The two cw spectra are shown in dotted (17 ns) and continuous (21 ns) black lines. The simulated changes in the correlation times have been chosen in such a way that the difference spectrum obtained by subtraction of

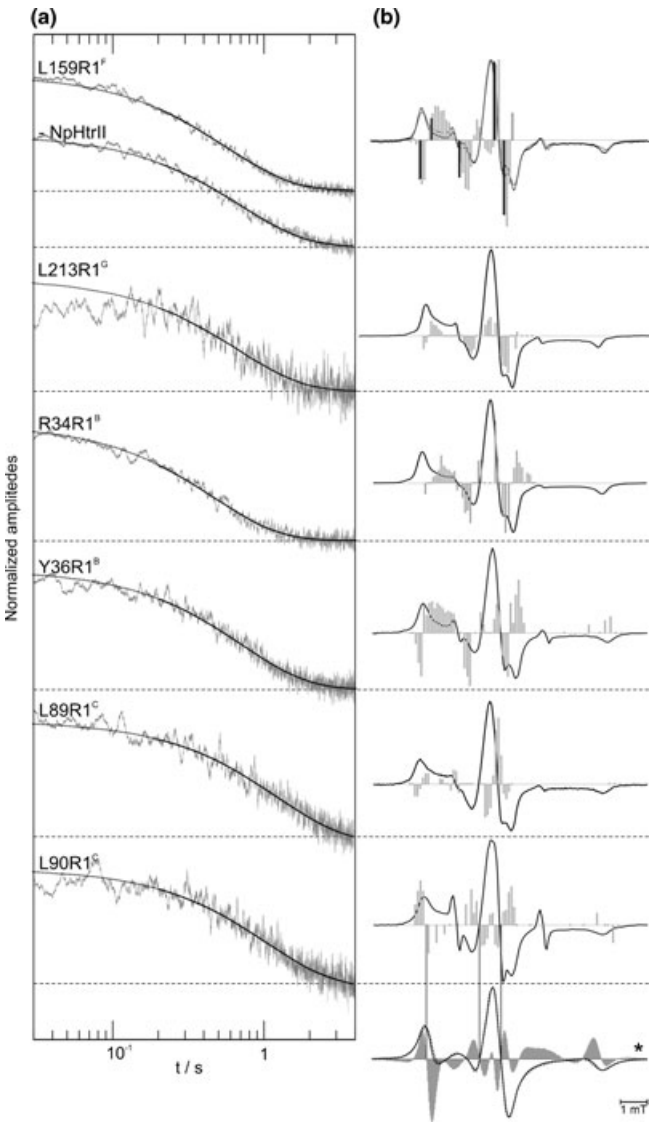

Figure 3. (a) Selected transient electron paramagnetic resonance (EPR) signal changes detected for the singly labeled *Np*SRII in complex with *Np*HtrII$_{157}$ reconstituted in purple membrane lipids (PML). The traces are shown in the logarithmic time scale (0.03–4 s), normalized to the maximal amplitude (noisy grey lines). The time constant of the lock-in amplifier was set to 5 ms. The mono-exponential fitting performed in the time range 0.2–4 s is superimposed (black line). For L159R1^{F} the transient trace obtained for *Np*SRII reconstituted in PML in the absence of *Np*HtrII$_{157}$ is also presented. The time constants obtained from the fittings are shown in Table 1. (b) The difference spectra obtained for the respective mutants are shown in stick representation superimposed to the first derivative cw EPR spectra detected concomitantly to the transient traces (black lines). Each grey stick represents the maximum amplitude of the EPR transient trace detected at the corresponding B-field position as obtained from the mono-exponential fitting. To allow better comparison the difference spectra have been arbitrarily scaled with respect to the cw spectra. For L89R1^{C} and L213R1^{G} relatively smaller amplitudes (30–50%) of the transient traces were obtained with respect to the other positions investigated. The cw spectrum of L159R1^{F} in the absence of the transducer protein (dotted line), together with the corresponding transient changes (black sticks at selected B-fields), are superimposed to the cw and difference spectra of L159R1^{F} in complex with *Np*HtrII$_{157}$. The low B-field and the central peak regions of the difference spectra reveal the fingerprint features to determine the changes in the spin label mobility. In the higher B-field region of the spectra the transient changes are almost less than the detection limit. For this reason no transient traces were detected for positions L159R1^{F}, L213R1^{G} and R34R1^{B} and only few points were detected for the other mutants. At the bottom of panel B, denoted by an asterisk, the simulated cw EPR spectra for correlation times of 21 ns (black line) and 17 ns (dotted line) are presented, superimposed to the difference spectrum obtained by subtraction of the 17 ns from the 21 ns spectrum (the area underneath the difference spectrum is colored in grey). The difference spectrum has been multiplied by 10. To facilitate the comparison with the experimental difference spectrum of L90R1^{C}, vertical lines are shown in correspondence with selected zero field crossings of the simulated spectrum.

Table 1. Time constants of the recovery of the *Np*SRII dark state and of the decay of the EPR transients, and A_{zz} values for the dark state.

	τ (500 nm)* [s]	τ (EPR)† [s]	A_{zz} (dark) [mT]
Wild type	0.6 ± 0.1	–	–
L159R1^{F}	0.7 ± 0.1	0.6 ± 0.1 (0.7 ± 0.2)‡	3.55 ± 0.01
L213R1^{G}	0.7 ± 0.1	0.7 ± 0.1	3.54 ± 0.01
R34R1^{B}	0.7 ± 0.1	0.5 ± 0.1	3.54 ± 0.01
Y36R1^{B}	0.7 ± 0.1	0.7 ± 0.1	3.55 ± 0.01
L89R1^{C}	0.9 ± 0.1	1.3 ± 0.1	3.63 ± 0.01§
L90R1^{C}	1.0 ± 0.1	1.1 ± 0.1	3.55 ± 0.01

EPR = electron paramagnetic resonance; PML = purple membrane lipids.
*The transient absorption changes after photoexcitation were recorded for the spin labeled mutants of *Np*SRII/*Np*HtrII$_{157}$ complexes reconstituted in PML. The traces were recorded at 296 K at the wavelength characteristic of the *Np*SRII ground state absorption (500 nm). Fitting of the recovery of the ground state was performed in the time range from 30 ms to 10 s with a mono-exponential function. Standard deviations in the order of 1% were obtained for the time constants, indicating the satisfactory quality of the mono-exponential fitting. The error presented in the table has been estimated based on sample heterogeneity and temperature fluctuations. †The EPR time constant is the average obtained from the mono-exponential fitting of the decays of the EPR transients in the time range from 200 ms to 4 s at six different B-field values where the difference spectrum exhibits maximum amplitudes. The estimated error is the calculated standard deviation. ‡EPR transient trace recorded for the receptor reconstituted in PML without the transducer moiety. §No changes in the A_{zz} values were detected for the majority of mutants investigated in the M-trapped state. For L89R1^{C} a decrease of 0.02 mT in the M-trapped state has been observed (see inset of Fig. 4).

the dotted spectrum from the black one has an amplitude of 10% of the maximum intensity of the cw spectrum. Larger differences in the correlation times would lead to difference spectra with larger amplitudes, which do not correlate with the intensities experimentally obtained. However, the spectral pattern would show similar positive/negative features even for larger differences in the correlation times.

The calculated difference spectrum reproduces satisfactorily the spectral features experimentally obtained for L90R1^{C}. The spectral pattern reveals the fingerprint positive peak followed by a negative peak in the low B-field region of the spectrum. Moreover, the narrow negative peak and the positive peak intersecting the cw spectrum at the zero crossing of the central resonance are also present, indicative of a decrease in mobility. By inverting the calculated difference spectrum, the fingerprint pattern expected for an increase in the spin label mobility is revealed. Comparison with the experimental difference spectra of L159R1^{F}, R34R1^{B} or Y36R1^{B}, for example, corroborates the interpretation given in the following paragraphs.

The difference spectra obtained for side chains L159R1^{F} and L213R1^{G}, located at the F–G and G–A helices interfaces, respectively, indicate an increase in the spin label side chain mobility upon light activation. As previously shown (7), the difference spectrum of L159R1^{F} is not influenced by the presence of the transducer. The comparison between the difference spectrum of L159R1^{F} in the *Np*SRII/*Np*HtrII$_{157}$ complex and selected transient amplitude changes (black sticks) obtained for the receptor alone reconstituted in PML is shown in Fig. 3b (upper spectra). Within the experimental errors, also the time course of the mobility changes of side chain L159R1^{F} is not influenced by the presence of the transducer (see Table 1). The EPR transient traces detected for L159R1^{F} were characterized by larger amplitudes with respect to L213R1^{G}, thus suggesting a major rearrangement occurring in the F–G rather than in the G–A interface. Assuming that during the photocycle helices F and G would be displaced relative to each other (both in the presence and absence of transducer) the increase in mobility of L159R1^{F} could be explained.

The two outwardly oriented side chains R34R1^{B} and L89R1^{C} showed as well difference spectra which can be correlated with an increase in the spin label side chain mobility. The amplitudes of the EPR transient traces detected for L89R1^{C} were smaller than those for R34R1^{B}. The features of the difference spectrum obtained for L89R1^{C} could arise both from an increase in the spin label mobility and from the slight decrease in the polarity of the spin label environment in the M-trapped state ($\Delta A_{zz}^{(\text{M-dark})} = -0.02$ mT, see Table 1 and Fig. 4). Such a small change in the A_{zz} is expected to produce a negative/positive fingerprint variation in the intensity of the low and high B-field peaks. However, the amplitude changes expected in the central peak of the spectrum in the case of a $\Delta A_{zz}^{(\text{M-dark})} = -0.02$ mT are negligible, as proven by a simulation of the difference spectrum (not shown). Thus, a simple change in polarity cannot explain the difference spectrum detected. On the other side, for all other positions investigated, neither changes in polarity nor appearance of dipolar broadening (which might occur for single mutants in the case of a light-induced oligomerization of the complexes) have been detected in the M-trapped state, thus leading to a straightforward interpretation of the difference spectra only in terms of changes of the spin label dynamics.

Considerably high amplitude changes were detected for both side chains which are oriented towards the interior of *Np*SRII (Y36R1^{B} and L90R1^{C}). This observation is indicative of relevant structural changes induced by light on the spin labels environment in the inner region of the receptor. The side chain Y36R1^{B} is characterized by an increase in the spin label mobility upon light excitation, whereas the spin label attached at L90^{C} was found to be involved in structural changes of its environment leading to a more restricted motion.

In a first attempt to investigate the kinetics of the transient decay of the EPR signal and to compare them to the optically detected changes in the absorption, a mono-exponential fit was performed (see Fig. 3a) both for the EPR transient traces and for the optical traces of the recovery of the ground state absorption (500 nm) recorded on the same samples. The comparison of the obtained time constants is presented in Table 1. Interestingly, different mutations lead to slight changes in the turnover rate of the *Np*SRII photocycle, as it was previously observed also for bacteriorhodopsin mutants (33). The optical traces of mutations affecting helices B, F and

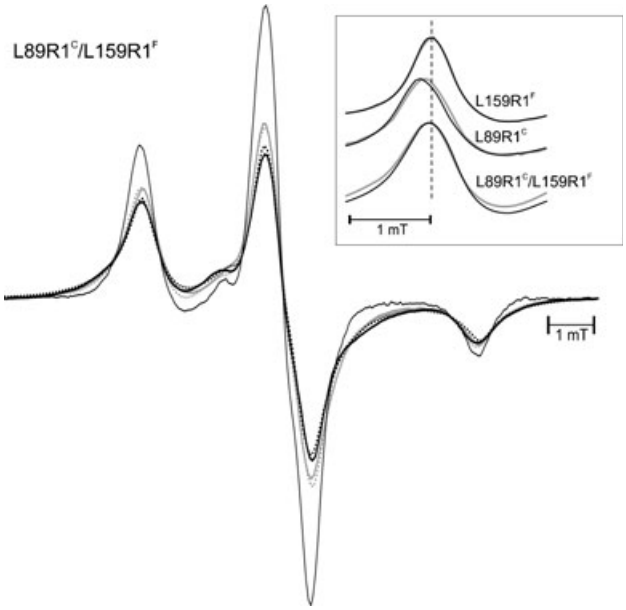

Figure 4. Spin normalized first derivative cw X-band electron paramagnetic resonance (EPR) spectra recorded at 170 K. The spectrum obtained from the sum of the two spectra of the singly labeled mutants L89R1^{C} and L159R1^{F} showing no dipolar line broadening is shown as reference (black thin line). The spectra of the corresponding double mutant in the dark (black thick line) and M-trapped (grey thick line) states are superimposed. The spectrum of the doubly labeled variant shows distinct line broadening in the dark state as visible from the decrease in the central peak intensity with respect to the reference spectrum. In the M-trapped state the line broadening decreases as visible from the increase of the central peak intensity compared with the dark state spectrum. The fittings of the simulated spectra to the experimental ones were performed with the DIPFIT program and presented as dotted lines. Inter-spin distances of 1.1 ± 0.2 nm for the dark state and 1.3 ± 0.2 nm for the M-trapped state (in the case of 100% yield of the trapping procedure) have been determined. The inset shows the normalized low B-field peaks of the low temperature EPR spectra obtained from the single mutants L159R1^{F} and L89R1^{C} and from the double mutant L89R1^{C}/L159R1^{F} in both dark (black) and M-trapped states (grey). The position of the peak maximum is indicative for the A_{zz} value. The vertical dashed line characterizes the position of the peak of the variant L159R1^{F} in the dark and in the M-trapped state (A_{zz} = 3.55 ± 0.01 mT). The shift to lower B-field values of the peaks of L89R1^{C} is clearly visible (A_{zz} = 3.63 ± 0.01 mT for the dark state and A_{zz} = 3.61 ± 0.01 mT for the M-trapped state). In case of the double mutant the intermediate position of the peak reveals an A_{zz} value of 3.57 ± 0.01 mT.

G do not reveal particular changes in the turnover rate of the *Np*SRII photocycle. On the other hand, slower decays seem to be associated with mutations involving residues L89^{C} and L90^{C} in helix C. The time constants obtained for the recovery of the structural changes monitored via EPR and for the recovery of the ground state absorption are highly correlated, once more confirming the relation between the light-induced optical and structural changes occurring in *Np*SRII.

Trapping of the M-state at low temperature: Polarity and distance changes

To investigate the polarity changes in the activated state, low temperature (170 K) cw EPR spectra were detected for the singly labeled mutants both in the dark-adapted and in the M-trapped states (see Materials and Methods and [14]). As an example, the low B-field peak of the rigid limit spectra for the two singly labeled mutants L89R1^{C} and L159R1^{F} and for the doubly labeled mutant L89R1^{C}/L159R1^{F} in the dark-adapted and in the M-trapped states are presented in the inset of Fig. 4.

The A_{zz} values obtained from the fitting of simulated spectra to the measured ones are summarized in Table 1. No changes in the polarity were detected between the dark and the M-trapped state for all positions investigated, except for L89R1^{C} where a decrease of 0.02 mT was observed. As already mentioned, this slight change in polarity of the spin label side chain environment might induce the negative and positive features in the low B-field region of the difference spectrum (Fig. 3b), but cannot, however, fully explain the pattern of the difference spectrum observed.

In general, the absence of dipolar broadening in the single mutants located at the outwardly oriented faces of helices B and C both in the dark and in the M-trapped states reveals that a possible interaction existing between adjacent complexes in membranes does not involve contacts of helices B or C to their counterparts, and that such an assembly is not induced by light excitation.

To investigate the changes in the interactions between helices C and F in the receptor upon light activation, a doubly labeled variant involving side chains L89R1^{C} and L159R1^{F} was engineered and investigated. Figure 4 shows the low temperature (170 K) spin normalized cw EPR spectra for the double mutant in the dark (black line) and M-trapped state (grey line) superimposed to the respective fittings and to the sum of the spectra of the two singly labeled variants (thin black line). As expected from the dipolar broadening already visible in the room temperature spectrum, considerable dipolar interaction allows to quantify the distance between the two side chains for the dark state (1.1 ± 0.2 nm). A significant decrease in the interaction between the two spins is observed for the M-trapped state, visible as an increase of the intensity of the central peak of the spin normalized spectrum. The distance increase has been proven to be fully reversible and reproducible. Fitting of the simulated powder spectrum to the experimental one gave a value of 1.3 ± 0.2 nm for the average inter-spin distance in the M-trapped state when considering a 100% yield in the M-trapping. However, the M-trapping procedure adopted leads to ~50% yield of the M-state (22). When considering in the fitting procedure that only 50% of the dipolar broadened spectrum arises from the new inter-spin distance characterizing the M-state, the increase in the distance could be estimated to be 0.4 nm. This evidence clearly shows that the close interaction existing between helices C and F in the dark-adapted state is loosened in the activated state.

DISCUSSION

Structural rearrangements occurring upon light excitation in the receptor/transducer interface, namely in helices F–G of the receptor and in helix TM2 of the transducer, have been elucidated during the last years by several biophysical techniques including accessibility assays, FTIR, FRET, molecular dynamics simulations, X-ray diffraction and EPR spectroscopy. The photocycle intermediates of *Np*SRII involved in the signaling mechanism have been suggested from several lines of research to coincide with the M_2 and O states (5,7,14,23).

Nevertheless, the nature of the structural changes leading to activation of the transducer still remains a matter of debate. A considerable number of different studies addressing this issue yielded partly contradictory results especially concerning the question, if a putative helix F outward bending motion is hindered by the bound transducer, thereby disputing its potential role in the signal transduction process.

In 2003, Spudich and coworkers published an FTIR analysis of the *Np*SRII and of the *Np*SRII/*Np*HtrII$_{147}$ fusion complex (the subscript denotes the residue at which the transducer has been truncated) reconstituted in phospholipids which revealed a set of altered bands suggesting structural changes occurring in the receptor which might be correlated to a helix F outward tilting (according to other FTIR results on BR), and which were altered by the presence of transducer (24). In 2006, also Kandori *et al*. (25) analyzed via FTIR the conformational alteration of PC reconstituted *Np*SRII (ppR) induced by light in the presence and absence of transducer. The results suggested that the interaction with the transducer impaired the opening of a cleft near helix F and that this impairment does not occur at low temperature or in the G83C/F mutants, which had already been shown to impair the transducer function (26). Similar conclusions were drawn from the fact that the transducer inhibits the bacteriorhodopsin-like light-driven ion pumping properties of *Np*SRII (27,28), assuming that proton uptake from the cytoplasmic side might be hampered due to inhibition of the opening of the proton channel. Finally, the most recent piece of evidence for such kind of inhibition of the helix F motion by the transducer turned out to be the crystal structure of the activated complex showing no indication for such conformational change of helix F, although the transducer seems to be activated (15). However, it should be mentioned that protein–protein contacts in the crystals involving the E–F loop might inhibit an outward bending motion of helix F. It should be noted in this context that Bergo *et al*. (29) and Furutani *et al*. (30) showed that the interaction interface between helices G and TM2, most prominently the hydrogen bond between Tyr199^{G} and Asn74^{TM2}, is affected by light excitation and that the recovery to the initial state follows the decay of the M and O intermediates. In contrast to that, all hydrogen bonds between helices F, G and TM2 were found intact in the late M crystal structure, indicating that conformational changes in the F–G–TM2 interface might be different in membranes and in the crystal.

On the other hand, a number of studies gave evidences for the presence of the helix F motion also in the presence of its cognate transducer. Spudich *et al*. (31) studied the fluorescent probe accessibility of cysteine residues introduced at several positions in the E–F loop of *Np*SRII in complex with *Np*HtrII$_{159}$ solubilized in DDM. Although they found that light activation decreased the accessibility of positions 151$^{E–F}$, 154$^{E–F}$ and 158^{F} in the complex but not in the receptor alone, they observed an increase in the Förster energy transfer between position 154$^{E–F}$ and the membrane-adjacent region of the transducer in the light activated state, in line with an outward movement of helix F upon light activation. In 2005, a computational analysis performed by Sato *et al*. (32) on the modeled M-state of *Np*SRII in complex with its transducer indicated the possibility to induce a large displacement of the cytoplasmic side of helix F and a concomitant clockwise rotation of TM2 by changing the protonation state of the amino acids involved in the retinal binding pocket. Significant evidences came also from previous site-directed spin labeling EPR investigations (5,7,8,14) which suggested an outward tilt of helix F occurring during the M_1 to M_2 transition also in the presence of the transducer.

In this work, new EPR evidences point to a detectable structural rearrangement of the entire cytoplasmic moiety of *Np*SRII upon light activation (helices B, C, F and G), and an increase in distance between helices C and F in the M-trapped state of the complex. This observation once more points to an outward movement of helix F as a putative interpretative model for the receptor activation.

Helices B and C

Structural rearrangements leading to changes in the spin label dynamics were detected both for the outwardly and inwardly oriented spin label side chains in helices B and C, indicating that the molecular switch activated by absorption of light in the core of the receptor (retinal binding site) induces an overall structural distortion also in the cytoplasmic exposed receptor region.

Both side chains Y36R1^{B} and L90R1^{C} are oriented towards the interior of *Np*SRII. While the spin label side chain in helix B shows a transient increase in the mobility, that one in helix C shows a transient decrease of the mobility. Comparing these results with previously published data on bacteriorhodopsin analogous mutants show similarities and distinct differences.

The analogous side chain of L90R1^{B} in *Np*SRII is L100R1$^{B}_{BR}$ in bacteriorhodopsin (the subscript denotes the side chains belonging to BR). No transient structural changes could be detected for this position in BR, however, the following residue V101R1$^{B}_{BR}$ showed a transient decrease in mobility (12), similarly to what is observed for L90R1^{B} in *Np*SRII. Light excitation seems to induce a more compact structural packing of the terminal part of helix C and the first residues of the C–D loop both in *Np*SRII and BR.

The analogous side chain of Y36R1^{B} in *Np*SRII is T46R1$^{B}_{BR}$ in bacteriorhodopsin. Contrarily to the side chain in *Np*SRII, T46R1$^{B}_{BR}$ was shown to undergo a transient decrease in the spin label side chain mobility upon light activation (33). The difference observed between the two analogous side chains might be explained by the fact that in bacteriorhodopsin, differently to what is suggested for sensory rhodopsin, the inward movement of helix G upon light activation could induce a decrease in mobility of the side chains located at the G–B interface. The increase in the mobility observed for Y36R1^{B} in *Np*SRII highlights the differences in the G–B interface in the two receptors.

Comparing the experimentally detected EPR transient changes of L90R1^{B} and Y36R1^{B} with the rearrangement occurring in the X-ray late M structure of *Np*SRII, we found that there is a slight side chain rearrangement taking place, especially in the R34-Y36 region. Moreover, the average B factor calculated for the neighboring residues of Y36 and L90 is increased by about 10 in the late M-state with respect to the dark structure. This could explain the observed increase in the mobility of Y36R1^{B}. On the contrary, the decrease in the mobility of L90R1^{B} cannot be inferred, neither from the increase in the B factors, nor from other structural rearrangements in the late M structure.

The side chains R34R1^{B} and L89R1^{C} reside on the outwardly oriented face of helices B and C, respectively. They both show an increase in the spin label mobility upon light activation. No analogous positions were investigated by EPR in bacteriorhodopsin. The present data indicate an increase in the dynamics of the cytoplasmic moiety of the two helices. This fact could be correlated with the already mentioned increase in the B factors in the late M-state X-ray structure of about 10 observed both for the backbone and the side chain atoms of the residues surrounding the two investigated positions. Interestingly, as shown in Fig. 5a, a relevant side chain rearrangement is detected in the late M structure for arginine 34, which is in agreement with transient mobility changes observed for the spin label attached at that side. Moreover, the side chain rearrangement observed for arginine 35 which is located at a C_β–C_β distance of 0.66 nm to the leucine 89, could also induce the changes in dynamics detected by the spin label attached at position 89.

Helices F and G

The data obtained in this work concerning the light-induced changes on the F–G helices interface as monitored by side chain L159R1^{F} are in line with the already proposed helix F motion. The experimentally obtained difference spectrum characterized by an increase in mobility of the spin label side chain is not influenced by the presence of the transducer, indicating that the light-induced structural changes occurring in the F–G interface do not depend on the interaction with the transducer. The cw EPR spectra detected in the presence and absence of the transducer in the dark-adapted state (Fig. 2) additionally indicate that the spectral features of L159R1^{F} derive only from intra molecular interactions. These results cannot be explained by the minor relative displacement of the F–G helices observed in the crystal structure of the late M-state. In the dark and late M-state structures, no side chain rearrangement is observed at position 159 and the slight relative shifts (<0.6 Å) of side chains located in helix G cannot account for the observed increase in the spin label mobility (Fig. 5b).

The minor transient changes in the spin label environment probed by side chain L213R1^{G}, located at the G–A interface, indicate a minor alteration of this interface upon light excitation which does not seem to be in line with the proposed ABG triad of helices relatively unaffected by light excitation. However, closer inspection of the L213 side chain and its environment in the dark-adapted and M-state crystal structures reveals local rearrangement of the native side chains, which might contribute to the minor variations monitored by the spin label probe dynamics (Fig. 5b).

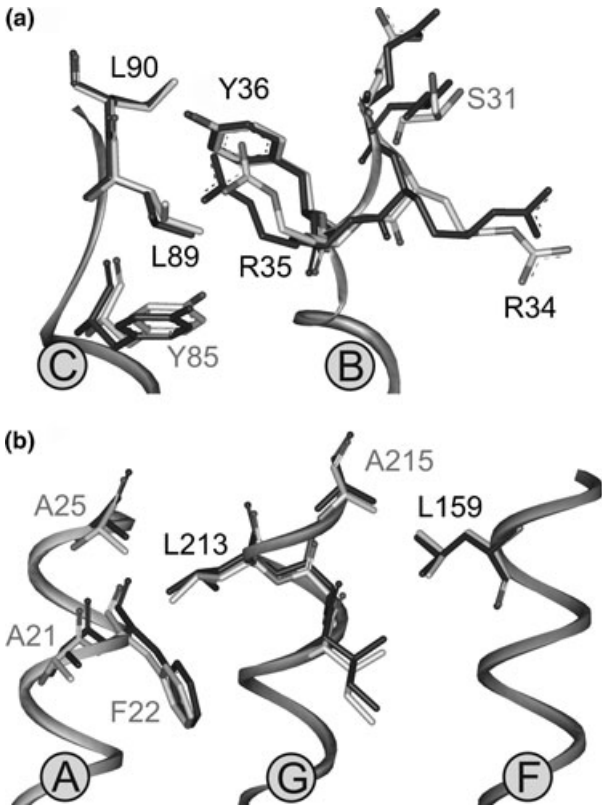

Figure 5. Comparison between the dark state and M-state crystal structures (pdb: 2F95) of the cytoplasmic ends of helices B and C (a) and helices A, F and G (b). Side chains are shown in stick representation (ground state: dark grey, M-state: light grey). For clarity the ribbon representation of the helices is just shown for the ground state structure.

Helix F movement

To further address the main question concerning the light-induced helix F movement in *Np*SRII as a cause for the receptor-transducer signal transfer, the doubly labeled mutant L89R1^{C}/L159R1^{F} was investigated. The distance between the spin labeled side chains determined by the fitting of the dark-adapted spectrum (1.1 ± 0.2 nm) agrees with the C_β–C_β distance of 1.08 nm obtained from the crystal structure of the dark state. A distance increase of up to 0.4 nm is suggested in the M-trapped state, which is on the contrary not observed in the late M crystal structure (C_β–C_β distance of 1.08 nm). This finding is in line with an outward displacement of helix F occurring in the activated M-state of *Np*SRII. An analogous double mutant involving side chains V101$^{C}_{BR}$ and A168$^{F}_{BR}$ was engineered in BR. An analogous distance increase of 0.1 nm was detected in the activated state which was explained by the outward movement of helix F (34).

At the moment, however, the fact that transient mobility changes are observed for both positions L159R1^{F} and L89R1^{C} in *Np*SRII, does not allow to definitely rule out the possibility that the relative displacement detected between helices F and C could be explained by an outward movement and/or rotation of helix C, or by a specific rearrangement of the spin label side chains after light excitation leading to a distance increase between the nitroxide groups. For the first case, no corroborating evidence exists in the late M crystal structure; for the second case, the absence of any rearrangement of the two native side chains seems to rule out the possibility of a large reorientation of the spin label moiety in the activated state. However, the spin labels attached to the engineered cysteines might be oriented differently with respect to the native side chains and consequently might be affected in a different way by the structural changes occurring.

CONCLUDING REMARKS

The data of the present work indicate for the first time how the cytoplasmic moiety of the receptor reconstituted with the transducer in its native environment is influenced by light activation. The spin label side chain is shown to be an efficient probe for even subtle molecular rearrangements. In fact, not only side chains located at the interface between helices or buried in the protein interior, but also side chains pointing outwardly experience transient changes upon light excitation which can be probed by the alteration of the spin label dynamics. The peculiar increase in mobility observed for $Y36R1^{B}$ seems to indicate that, contrarily to BR, an inward movement of helix G does not occur in *Np*SRII. (Helix G is already slightly inwardly bent in the dark state of sensory rhodopsin with respect to BR [8]). On the other side, the similar decrease in mobility detected for the C–D loop both in *Np*SRII and BR could reinforce the concept that similarities in the light excitation response exist in this part of the receptors.

Concerning the question whether helix F exhibits an outward bending motion upon light activation of the *Np*SRII/*Np*HtrII$_{157}$ complex, the data obtained in this work with the engineered doubly labeled mutant are in line with the previously proposed outward tilting of helix F. Nevertheless, the observation of possible transducer activation without the conformational change of helix F as observed in the crystal structure of the late M-state, might question the active role of helix F in the signal transduction process. Taking into account the discrepancies concerning the preservation of hydrogen bonds in the G–TM2 interface, one of the possibilities to be discussed and probed would be a two-step process, in which the relative shift observed in the X-ray structures between helices F and G is the first step in transducer activation, leading to a "pre-activated" state, still exhibiting an unimpaired Y199-N74 hydrogen bond linkage. The second step would then be the outward tilt of helix F resulting in further conformational changes of the transducer, thereby disrupting the hydrogen bond, and leading to the active state.

To fully unravel the structural changes occurring upon light excitation in *Np*SRII and to validate the crystallographic data of the late M-state, the creation and investigation of several double mutants is required. Detailed correlation of the transient EPR detected structural changes and the optically detected absorption changes will help unraveling the time course of the molecular events. Application of molecular dynamics simulation approaches performed at different spin label sites both in the dark and late M-state structures will be also employed.

Acknowledgements—This work was supported by the Deutsche Forschungsgemeinschaft (SFB 431/P18 H.-J.S.) and the Max Planck Society (M.E.).

REFERENCES

1. Spudich, J. L., C.-S. Yang, K.-H. Jung and E. N. Spudich (2000) Retinylidene proteins: Structures and functions from archaea to humans. *Annu. Rev. Cell Dev. Biol.* **16**, 365–392.
2. Schäfer, G., M. Engelhard and V. Müller (1999) Bioenergetics of the archaea. *Microbiol. Mol. Biol. Rev.* **63**, 570–620.
3. Landau, E. M., E. Pebay-Peyroula and R. Neutze (2003) Structural and mechanistic insight from high resolution structures of archaeal rhodopsins. *FEBS Lett.* **555**, 51–56.
4. Spudich, J. L. and H. Luecke (2002) Sensory rhodopsin II: Functional insights from structure. *Curr. Opin. Struct. Biol.* **12**, 540–546.
5. Klare, J. P., V. I. Gordeliy, J. Labahn, G. Büldt, H. J. Steinhoff and M. Engelhard (2004) The archaeal sensory rhodopsin II/transducer complex: A model for transmembrane signal transfer. *FEBS Lett.* **564**, 219–224.
6. Chizhov, I., G. Schmies, R. P. Seidel, J. R. Sydor, B. Lüttenberg and M. Engelhard (1998) The photophobic receptor from *Natronobacterium pharaonis*: Temperature and pH dependencies of the photocycle of sensory rhodopsin II. *Biophys. J.* **75**, 999–1009.
7. Wegener, A. A., I. Chizhov, M. Engelhard and H.-J. Steinhoff (2000) Time-resolved detection of transient movement of helix F in spin-labelled pharaonis sensory rhodopsin II. *J. Mol. Biol.* **301**, 881–891.
8. Klare, J. P., E. Bordignon, M. Engelhard and H.-J. Steinhoff (2004) Sensory rhodopsin II and bacteriorhodopsin: Light activated helix F movement. *Photochem. Photobiol. Sci.* **3**, 543–547.
9. Subramaniam, S. and R. Henderson (2000) Molecular mechanism of vectorial proton translocation by bacteriorhodopsin. *Nature* **406**, 653–657.
10. Luecke, H., B. Schobert, H.-T. Richter, J.-P. Cartailler and J. K. Lanyi (1999) Structural changes in bacteriorhodopsin during ion transport at 2 Angstrom resolution. *Science* **286**, 255–260.
11. Sass, H. J., G. Büldt, R. Gessenich, D. Hehn, D. Neff, R. Schlesinger, J. Berendzen and P. Ormos (2000) Structural alterations for proton translocation in the M state of wild-type bacteriorhodopsin. *Nature* **406**, 649–653.
12. Rink, T., M. Pfeiffer, D. Oesterhelt, K. Gerwert and H.-J. Steinhoff (2000) Unraveling photoexcited conformational changes of bacteriorhodopsin by time resolved electron paramagnetic resonance spectroscopy. *Biophys. J.* **78**, 1519–1530.
13. Steinhoff, H.-J., A. Savitsky, C. Wegener, M. Pfeiffer, M. Plato and K. Möbius (2000) High-field EPR studies of the structure and conformational changes of site-directed spin labeled bacteriorhodopsin. *Biochim. Biophys. Acta* **1457**, 253–262.
14. Wegener, A. A., J. P. Klare, M. Engelhard and H.-J. Steinhoff (2001) Structural insights into the early steps of receptor-transducer signal transfer in archaeal phototaxis. *EMBO J.* **20**, 5312–5319.
15. Moukhametzianov, R., J. P. Klare, R. Efremov, C. Baeken, A. Göppner, J. Labahn, M. Engelhard, G. Büldt and V. I. Gordeliy (2006) Development of the signal in sensory rhodopsin and its transfer to the cognate transducer. *Nature* **440**, 115–119.
16. Bordignon, E., J. P. Klare, M. A. Doebber, A. A. Wegener, S. Martell, M. Engelhard and H. J. Steinhoff (2005) Structural analysis of a HAMP domain: The linker region of the phototransducer in complex with sensory rhodopsin II. *J. Biol. Chem.* **280**, 38767–38775.
17. Freed, J. H. (1976) Theory of slow tumbling ESR spectra for nitroxides. In *Spin Labeling: Theory and Applications* (Edited by L. J. Berliner), pp. 83–91. Academic Press, New York.
18. Steinhoff, H.-J., N. Radzwill, W. Thevis, V. Lenz, D. Brandenburg, A. Antson, G. Dodson and A. Wollmer (1997) Determination of interspin distances between spin labels attached to insulin: Comparison of electron paramagnetic resonance data with the X-ray structure. *Biophys. J.* **73**, 3287–3298.
19. Plato, M., H.-J. Steinhoff, C. Wegener, J. T. Törring, A. Savitsky and K. Möbius (2002) Molecular orbital study of polarity and hydrogen bonding effects on the g and hyperfine tensors of site directed NO spin labelled bacteriorhodopsin. *Mol. Phys.* **100**, 3711–3721.
20. Wegener, C., A. Savitsky, M. Pfeiffer, K. Möbius and H.-J. Steinhoff (2001) High-field EPR-detected shifts of magnetic tensor components of spin label side chains reveal protein conformational changes: The proton entrance channel of bacteriorhodopsin. *Appl. Magn. Reson.* **21**, 441–452.
21. Hippler-Mreyen, S., J. P. Klare, A. A. Wegener, R. Seidel, C. Herrmann, G. Schmies, G. Nagel, E. Bamberg and M. Engelhard (2003) Probing the sensory rhodopsin ii binding domain of its cognate transducer by calorimetry and electrophysiology. *J. Mol. Biol.* **330**, 1203–1213.
22. Balashov, S. P., M. Sumi and N. Kamo (2000) The M intermediate of *Pharaonis* phoborhodopsin is photoactive. *Biophys. J.* **78**, 3150–3159.

23. Yan, B., T. Takahashi, R. Johnson and J. L. Spudich (1991) Identification of signaling states of a sensory receptor by modulation of lifetimes of stimulus-induced conformations: The case of sensory rhodopsin II. *Biochemistry* **30**, 10686–10692.
24. Bergo, V., E. N. Spudich, J. L. Spudich and K. J. Rothschild (2003) Conformational changes detected in a sensory rhodopsin II-transducer complex. *J. Biol. Chem.* **278**, 36556–36562.
25. Kamada, K., Y. Furutani, Y. Sudo, N. Kamo and H. Kandori (2006) Temperature-dependent interactions between photoactivated *Pharaonis* phoborhodopsin and its transducer. *Biochemistry* **45**, 4859–4866.
26. Yang, C.-S. and J. L. Spudich (2001) Light-induced structural changes occur in the transmembrane helices of the *Natronobacterium pharaonis* HtrII transducer. *Biochemistry* **40**, 14207–14214.
27. Sudo, Y., M. Iwamoto, K. Shimono, M. Sumi and N. Kamo (2001) Photo-induced proton transport of *Pharaonis* phoborhodopsin (sensory rhodopsin II) is ceased by association with the transducer. *Biophys. J.* **80**, 916–922.
28. Schmies, G., M. Engelhard, P. G. Wood, G. Nagel and E. Bamberg (2001) Electrophysiological characterization of specific interactions between bacterial sensory rhodopsins and their transducers. *Proc. Natl Acad. Sci. USA* **98**, 1555–1559.
29. Bergo, V., E. N. Spudich, K. J. Rothschild and J. L. Spudich (2005) Photoactivation perturbs the membrane-embedded contacts between sensory rhodopsin II and its transducer. *J. Biol. Chem.* **280**, 28365–28369.
30. Furutani, Y., K. Kamada, Y. Sudo, K. Shimono, N. Kamo and H. Kandori (2005) Structural changes of the complex between *Pharaonis* phoborhodopsin and its cognate transducer upon formation of the M photointermediate. *Biochemistry* **44**, 2909–2915.
31. Yang, C. S., O. Sineshchekov, E. N. Spudich and J. L. Spudich (2004) The cytoplasmic membrane-proximal domain of the HtrII transducer interacts with the E–F loop of photoactivated natronomonas pharaonis sensory rhodopsin II. *J. Biol. Chem.* **279**, 42970–42976.
32. Sato, Y., M. Hata, S. Neya and T. Hoshino (2005) Computational analysis of the transient movement of helices in sensory rhodopsin II. *Protein Sci.* **14**, 183–192.
33. Rink, T., J. Riesle, D. Oesterhelt, K. Gerwert and H. J. Steinhoff (1997) Spin-labeling studies of the conformational changes in the vicinity of D36, D38, T46, and E161 of bacteriorhodopsin during the photocycle. *Biophys. J.* **73**, 983–993.
34. Radzwill, N., K. Gerwert and H.-J. Steinhoff (2001) Time-resolved detection of transient movement of helices F and G in doubly spin-labeled bacteriorhodopsin. *Biophys. J.* **80**, 2856–2866.